Journal of Colloid and Interface Science 658 (2024) 903–912

Contents lists available at ScienceDirect

Journal of Colloid And Interface Science

journal homepage: www.elsevier.com/locate/jcis

An all-fiber system biosensor for trace β-lactam antibiotics detection enhanced by functionalized microfiber and fiber bragg grating

Dandan Sun [a,*], Zifan Hou [a], He Yan [a], Yukun Yang [b], Guanjun Wang [c], Jizhou Wu [a,d], Jie Ma [a,d,*]

[a] School of Physics and Electronic Engineering, Shanxi University, Taiyuan, China
[b] School of Life Science, Shanxi University, Taiyuan 030006, China
[c] School of Information and Communication Engineering, Hainan University, Haikou 570228, China
[d] Collaborative Innovation Center of Extreme Optics, Shanxi University, Taiyuan, China

GRAPHICAL ABSTRACT

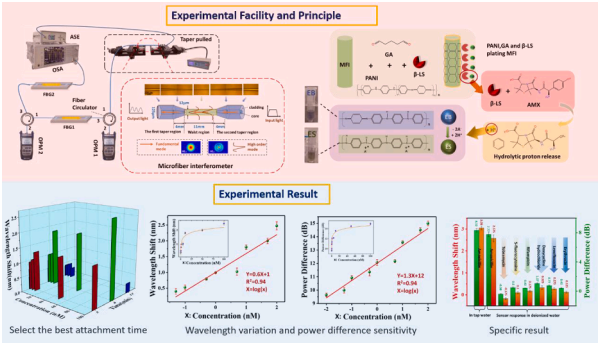

ARTICLE INFO

Keywords:
Microfiber interferometer
Fiber gratings
β-lactamase
Polyaniline
Amoxicillin

ABSTRACT

An all-fiber-optic system for rapid detection of antibiotic concentration, based on an optical enzyme biosensor with microfiber interferometer (MFI) and fiber gratings (FBGs) power variation, is proposed and experimentally validated. During the experiment, β-lactamase(β-LS) is fixed on the polyaniline (PANI)-coated optical fiber by cross-linking through glutaraldehyde (GA) covalent bonding. β-LS can hydrolyze β-lactam antibiotics to generate acidic by-products that transform polyaniline from the form of the emerald base to emerald salt, which results in the surface refractive index (RI) variation of MFI, to convert MFI wavelength and FBGs power macroscopic change for feedbackingly detecting the concentration of β-lactam antibiotics. The detection of amoxicillin (AMX) in deionized water at concentrations in the range of 0.01–100 nM resulted in a wavelength change sensitivity of 0.6 nm/nM, and FBGs power difference change sensitivity of 1.3 dB/nM, with a detection limit LOD = 0.04 nM in real food and urine samples. The sensing system by the same calibration technique can detect antibiotic concentrations in different substances (tap water, milk and artificial urine). This developed all-fiber-optic system can be used as a rapid solution for the measurement of β-lactam antibiotic residues in food and the environment.

* Corresponding authors.
E-mail addresses: sundd@sxu.edu.cn (D. Sun), mj@sxu.edu.cn (J. Ma).

https://doi.org/10.1016/j.jcis.2023.12.118
Received 11 October 2023; Received in revised form 5 December 2023; Accepted 19 December 2023
Available online 22 December 2023

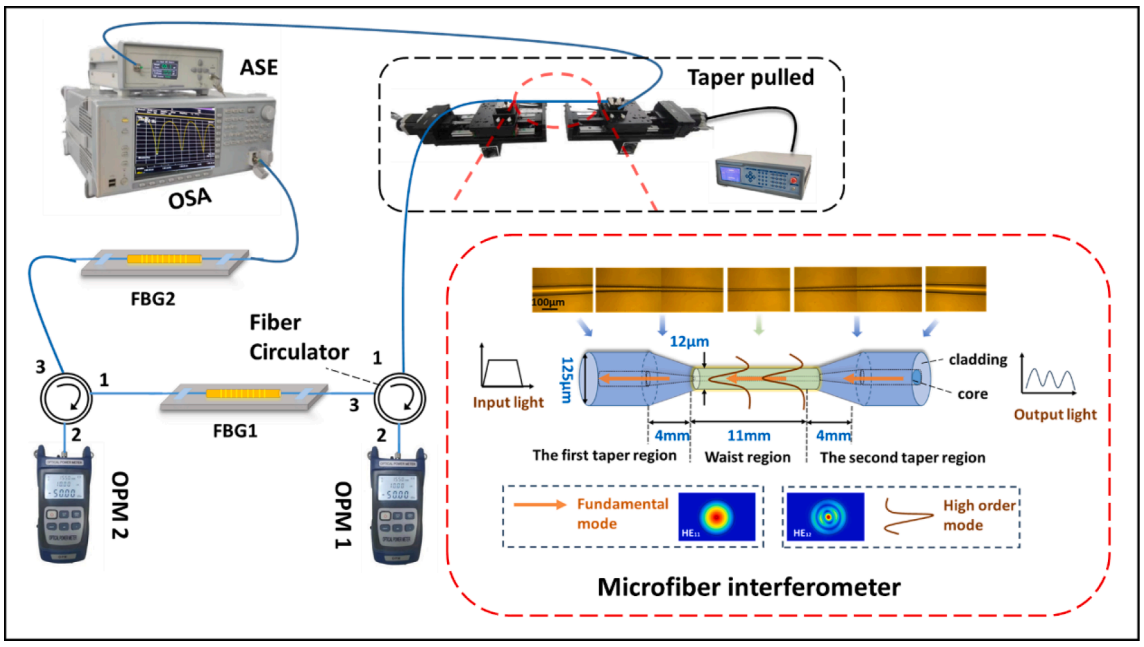

Fig. 1. Experimental equipment and the fabrication of microfiber interferometer. (Illustration: Structure and parameters of the interferometer.).

1. Introduction

Antibiotics are a class of secondary metabolites produced by microorganisms or higher plants and animals in the course of their lives that have anti-pathogenic or other activity and can interfere with the developmental functions of other living cells chemical substances [1]. With the gradual increase in the use of antibiotics worldwide in recent years to improve productivity, yield and quality of livestock, the widespread use of antibiotics is an important factor in the increase of antimicrobial resistance[2]. Most organizations have called for the reduction or elimination of antibiotic use in the compound sector and banning antibiotics in edible products such as pigs, chickens, and cattle [3]. Recent studies have found that antibiotics have been detected in hospital waste [4], industrial wastewater [5], and human domestic wastewater at concentrations that exceed the safe use of antibiotics. However, in the absence of stable antibiotic detection, this poses a significant safety concern for the safe drinking of water quality.

At this stage of existence antibiotic detection usually uses solid phase extraction, concentration, followed by chromatographic separation and finally mass spectrometry. This process requires the use of complex analytical instruments and specialized operators, but these costs are often unaffordable for small and medium-sized enterprises, especially in developing countries [6]. Immunoassay and bioinhibition-based kits can detect antibiotic residues in food, and although they are inexpensive, most of them do not provide accurate measurements and do not have adequate detection limits [7]. Immunoassay techniques contain radioimmunoassay [8], enzyme-linked immunosorbent assays [9], and immunosensors [10], which do not require tedious steps, are low-cost and fast detection, but they only provide preliminary screening of antibiotics and do not provide accurate detection. Some classical methods have high detection accuracy, but they are complicated to operate and require expensive costs. This process requires the use of sophisticated analytical instruments and specialized operators.

Some methods for detecting antibiotic concentrations have been reported in recent years in articles, such as electrochemical methods [1112], colorimetric methods [1314], and photoelectric methods [15]. Yu, Z. G. et al. used methylene blue-modified aptamer probes for the detection of ampicillin antibiotics using an electrochemical approach [11]. Wu, Y. et al. used an electrochemical approach based on single graphene nanosheets preabsorbed with hematein/ionic liquids/ penicillinase for the detection of penicillin [12]. Ain, N.U. et al. reported a colorimetric detection based on quercetin-coated silver nanoparticles to selectively identify amoxicillin [13], and Sethu, N. et al. established an iron-dependent lipid peroxidation to develop a rapid and sensitive colorimetric assay for detecting aminoglycoside antibiotics [14]. Guliy, O. I. et al. used a system consisting of Pseudomonas aeruginosa TSh-18 and a photoelectric sensor for the detection of ampicillin [15]. The above approach is simpler to operate than the classical detection methods, but the detection accuracy and detection limits do not meet the requirements of detection. With the continuous development of fiber optic sensing technology, it provides a new idea for the detection of antibiotics due to the advantages of low price, simple operation, and high sensitivity. For example, Ayankojo, A. G. et al. used surface plasmon resonance, a label-free sensing platform with molecularly imprinted polymer as a robust recognition element for real-time detection of antibiotics [16]. Gao, D. et al. reported a sensor based on microstructured hollow fibers with a suspended core fabricated using optical fluid Raman spectroscopy for the detection of ceftriaxone [17]. Nag, P. et al. reported a sensor attached β-LS to a U-shaped optical fiber to utilize the hydrolysis properties of β-LS for detecting antibiotics [18]. In recent years, microfiber has been gradually applied as a tool for detecting specific substances by virtue of its extremely low optical transmission loss, high core-cladding refractive index difference, and a large percentage of evanescent wave transmission. The method of combining materials with optical fiber to form a fiber sensor operates simply operationally, is efficient, easy to implement, which can be specific for the detection of the substance, and provides a novel platform for the detection of antibiotics.

In this work, we design a PANI and β-LS coated all-fiber biosensors optic sensor with MFI and FBGs power variations, which can detect changes in the concentration of antibiotics (amoxicillin) due to changes in the external refractive index caused by strong decaying fields. The MFI wavelength RI sensitivity is 952.7 nm/RIU and the variation of the power difference of the normalized FBG1-FBG2 under different RI conditions with the power difference RI sensitivity of 4199.6 dB/RIU and small cross-sensitizing properties. The experimental results show that the sensitivity to detect wavelength change and power difference change of AMX in the range of 0.01–100 nM is 0.6 nm/nM and 1.3 dB/nM, respectively. The detection limit (LOD) obtains 0.04 nM in real food and urine samples. Further tests are conducted on the sensing system for

detecting antibiotic concentrations in different substances (tap water, milk and artificial urine). The sensor provides a strong and favorable platform for the detection of β-lactam antibiotics in the measurement of beta-lactam residues in food and the environment.

2. Materials and methods

2.1. Reagents and instruments

Aniline (≥99.5 %), phosphoric acid (AR, ≥85 wt% in H_2O), ammonium persulfate (AR, 98.5 %), glutaraldehyde (25 % in H_2O), Milk (procured from local mall), artificial urine (procured from Regan Bio, pH = 7). β-lactamase (Lyophilized powder, 10 million units), amoxicillin (≥99 %), erythromycin (Biotechnology grade), levofloxacin (98 %), doxycycline hydrochloride (ACS grade, 95–102 %), rifampicin (97 %), 5-fluorocytosine (99 %), tobramycin (potency: ≥900μG/mg, 98 %), are purchased from Shanghai Maclean Biochemical Technology Co. (Shanghai China). Deionized water (Resistivity > 18 MΩ·cm) is used for dissolution in all experiments.

Optical equipment included an amplified spontaneous emission light source (ASE, MClight, China), optical spectrum analyzer (OSA, Anritsu MS9740A, Japan), Optical power meter (OPM, China), Fiber Optic Circulator. Auxiliary instruments included a fiber optic fusion splicer (Fujikura FSM-60S, Japan), Taper pulled (ZOLIX, MC600, China), digital refractometer (Brix/RI-Check Reichert, USA), optical microscope (Caikon DMM-200C), and temperature chamber (NG6000-2). The equipment used for characterization includes a Field emission scanning electron microscope (Hitachi SU8100, Japan), Fourier Infrared Spectroscopy (Bruker ALPHAII, Germany), and High-resolution Mass spectrometry (Waters 1515, solan X70 FT-MS, America).

2.2. Experimental setup and fabrication of microfiber interferometer

Fig. 1 shows the experimental setup and the fabrication of the microfiber interferometer (MFI). The light is emitted from the ASE (range 1528–1603 nm, power 10 mW), passes through the MFI, is transmitted to two FBGs, and finally detected by the OSA (range 600–1700 nm, resolution 0.03 nm). By using two fiber circulators to access the two OPMs it is possible to monitor the power changes of the FBGs in real-time. The fiber diameter is gradually reduced from 125 μm to 12 μm by heating with a butane flame gun (8S for the photosensitive fiber part) and automatic uniform stretching using a motion controller. Set the operating parameters of the motion controller to avoid experimental errors, in which the pulling cone speed is 2 mm/s, the acceleration is 5 mm/s^2, the maximum speed is 9 mm/s, and the pulling cone distance is 19 mm, and finally a stable microfiber interferometer is prepared. The inset part (red dotted line) is the schematic of the structural parameters of the MFI. The upper part is an isometric magnification taken using an optical microscope, and the lower part shows the specific parameters of the MFI. Consists of two transition regions with a length of 4 mm and a Waist region with a length of 11 mm and a diameter of 12 μm.

2.3. Sensing principle

2.3.1. Principle of microfiber interferometer

The MFI is prepared by fused pulling taper as shown in Fig. 1 (inset). Due to the thinning of the fiber diameter in the middle region of the ultrafine fiber sensor, the core and cladding diameters are also decreasing. When the incident light enters the ultrafine fiber, a part of the light continues to propagate along the core, and the other part of the light enters the tapered transition region of the fiber to propagate. Under the action of the evanescent field, a part of the core modes can be coupled to the envelope of the tapered region with a smaller diameter, thus exciting the higher-order modes in the envelope [19 20]. In the full-waist region, the fundamental core and envelope modes propagate simultaneously, which mainly propagating the fundamental (HE_{11}) and higher-order modes (HE_{12}) [21]. Fig. 1 (inset, below) shows the transverse electric field amplitude distributions of HE_{11} and HE_{12} in the main interferential modes. As the light propagates into the second tapered transition region, the fundamental core and cladding modes couple, reorganize, and produce an interferential pattern [22]. When the external refractive index (RI) changes, the interferential wave appears blue-shifted or red-shifted, and the sensitivity at this point can be used to evaluate the RI performance of the sensor. It can be expressed as [21 23]

$$\frac{d\lambda}{dR_{sm}} = \frac{\lambda}{\Gamma}\left(\frac{1}{\Delta R_{ccm}}\frac{d\Delta R_{ccm}}{dR_{sm}}\right) \tag{1}$$

where $\Gamma = 1 - \frac{\lambda}{\Delta R_{ccm}}\frac{d\Delta R_{ccm}}{d\lambda}$ is the dispersion factor, and the calculated value is negative. λ is the wavelength of the dip angle in the emission spectrum, and $\frac{d\Delta R_{ccm}}{d\lambda}$ is the refractive index-dependent change induced by a small change of wavelength. R_{sm} is the RI of the surrounding medium. $\frac{d\Delta R_{ccm}}{dR_{sm}}$ is the RI of the external refractive index effect. From Equation (1), the MFI with small diameter and small index difference has high sensitivity because the index increment of HE_{12} mode is larger than that of HE_{11} mode with the increase of external RI [21], The ΔR_{ccm} is the difference between the validity of the core and cladding modes. R_{co} and R_{cl} are the RI of the microfiber core and cladding. The relationship between them can be expressed as

$$\Delta R_{ccm} = R_{co} - R_{cl} \tag{3}$$

$$d\Delta R_{ccm} = \Delta R_{ccm2} - \Delta R_{ccm1} \tag{4}$$

The Finite Element Analysis software shows that the refractive index of the surrounding air is 1. When the RI difference increases due to the influence of small changes in the wavelength or refractive index of the surrounding air, ΔR_{ccm} the refractive index increment of the HE_{12} mode is larger than that of the HE_{11} mode, and therefore $\frac{d\Delta R_{ccm}}{dR_{sm}}$ is negative, and the discretization factor Γ is also negative. The results show that the wavelength redshifts with increasing RI [21].

2.3.2. Detection principle of fiber bragg gratings

When the RI around the changes and the wavelength is red-shifted, while the wavelength of the FBG stays constant, and the reflective intensities of the two FBGs change in opposite trends. The intensity difference of the two FBGs is more sensitive to RI than a single reflected intensity, which can be written as [24]

$$\Delta I = I_1 - I_2 = \int_{-\infty}^{\infty} S(\lambda)\cdot T_1(\lambda-\Delta\lambda)\cdot R_1\cdot\delta(\lambda-\lambda_1)d\lambda$$

$$-\int_{-\infty}^{\infty} S(\lambda)\cdot T_2(\lambda-\Delta\lambda)\cdot R_2\cdot\delta(\lambda-\lambda_2)d\lambda$$

$$= R_1 S(\lambda_1)T_1(\lambda_1-\Delta\lambda) - R_2 S(\lambda_2)T_2(\lambda_2-\Delta\lambda) \tag{5}$$

where ΔI is the differential intensity of the two FBGs. I_1 and I_2 are the reflected intensities of FBG1 and FBG2, $S(\lambda)$ is the power spectral density function of the light source. $T_1(\lambda)$ and $T_2(\lambda)$ are the initial transmission spectral functions of the two linear regions of the MFI. λ_1 and λ_2 are the wavelengths of FBG1 and FBG2, and $\delta(\lambda)$ is the wavelength shift of the MFI induced by the change of external index of refraction. R_1 and R_2 are the reflection coefficients of FBG1 and FBG2, $\delta(\lambda-\lambda_1)$ is the unit pulse function, and $R_1\cdot\delta(\lambda-\lambda_1)$ and $R_2\cdot\delta(\lambda-\lambda_2)$ are the reflection spectral functions of the FBGs, which is described as a pulse function because the bandwidth of the FBGs is smaller than that of the MFI. Since $\delta(\lambda)$ is related to the RI, the measurement of the RI can be done by calculating the differential intensity of the two FBGs. In addition, the wavelengths of the FBGs and FMI change less with increasing temperature, which minimizes the temperature dependence of the RI measurement [2526]. Two FBGs are used as line markers, and the intensity of their reflection peaks reflected the intensity of the FMI spectrum in real time. The

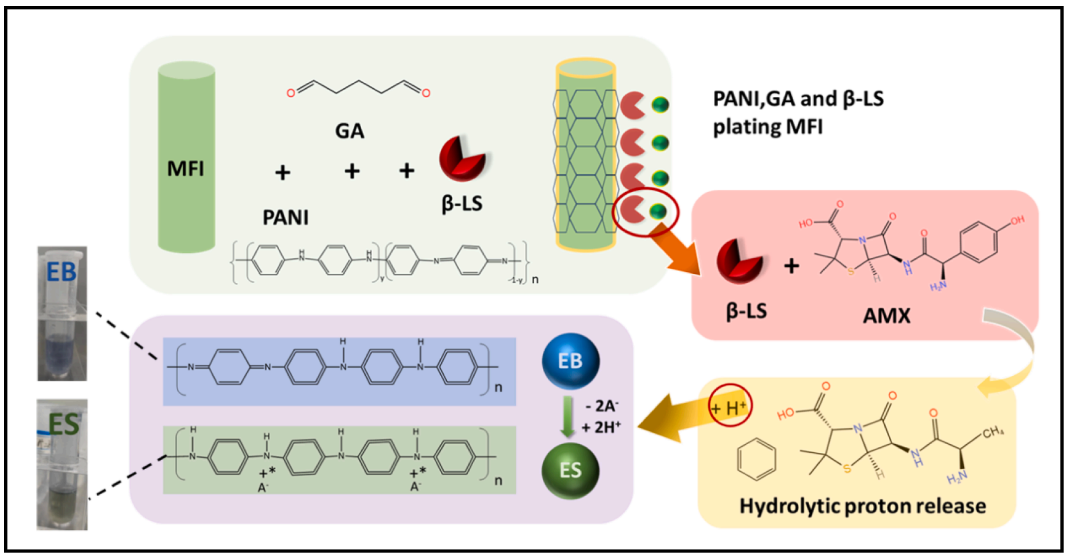

Fig. 2. Schematic diagram of the biosensor detection principle.

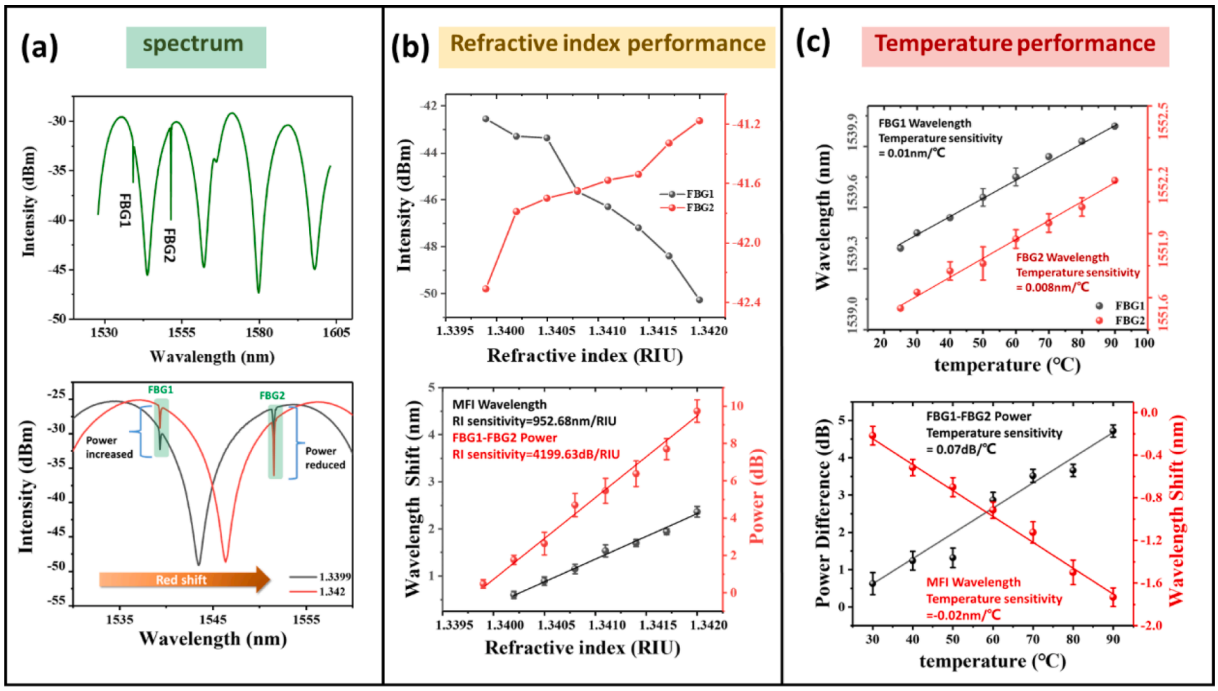

Fig. 3. (a) The Spectrum of Microfiber interferometer and fiber grating power variations in the all-fiber system (b) RI response performance of the all-fiber system (c) Temperature response performance of the all-fiber system.

estimation accuracy of the total spectral shift is improved by utilizing two FBGs. When the output spectrum is red-shifted, the intensity of the fiber grating peaks changes accordingly. When used to normalize ΔI(FBG1-FBG2), the change in the power of the FBGs can be utilized to detect the change in specific substance concentration [18].

2.3.3. *Biofiber sensor detection principle*

We designed a PANI-modified fiber optic biosensor for the detection of β-LS antibiotics. As shown in Fig. 2 (green). Aniline is polymerized into PANI by polymerization in an acidic environment and subsequently functionalized into the tapered region of the MFI. β-LS is immobilized onto the PANI-coated optical fiber by using the glutaraldehyde (GA) covalent cross-linking method with the help of aldehyde groups at both ends. Since the abrupt field of the MFI can extend to the outer surface of the cladding, this means that the abrupt field can be used to detect small changes in the effective RI of the microfiber surface with the binding of amoxicillin (AMX) to the cladding [27]. As shown in Fig. 2 (red and yellow), when β-LS bind to AMX, these β-LS are serine hydrolases in which the hydroxyl group of a serine amino acid attacks the carbon-based carbon of the amide bond in the β-LS ring of the antibiotic (amoxicillin) to form an acylase intermediate, which is subsequently hydrolyzed to form various degradation products and a proton H [28]. As shown in Fig. 2 (purple), the protons and acidic products produced by hydrolysis lead to a change in the local pH in the vicinity of the PANI, which protonates the PANI nanofibers and alters their charge distribution, resulting in the transition of the PANI from the emeraldine base (EB) to the emeraldine salt (ES) oxidation state [29]. As shown in Fig. 2 (left), the color change of the sphere reveals the experimental

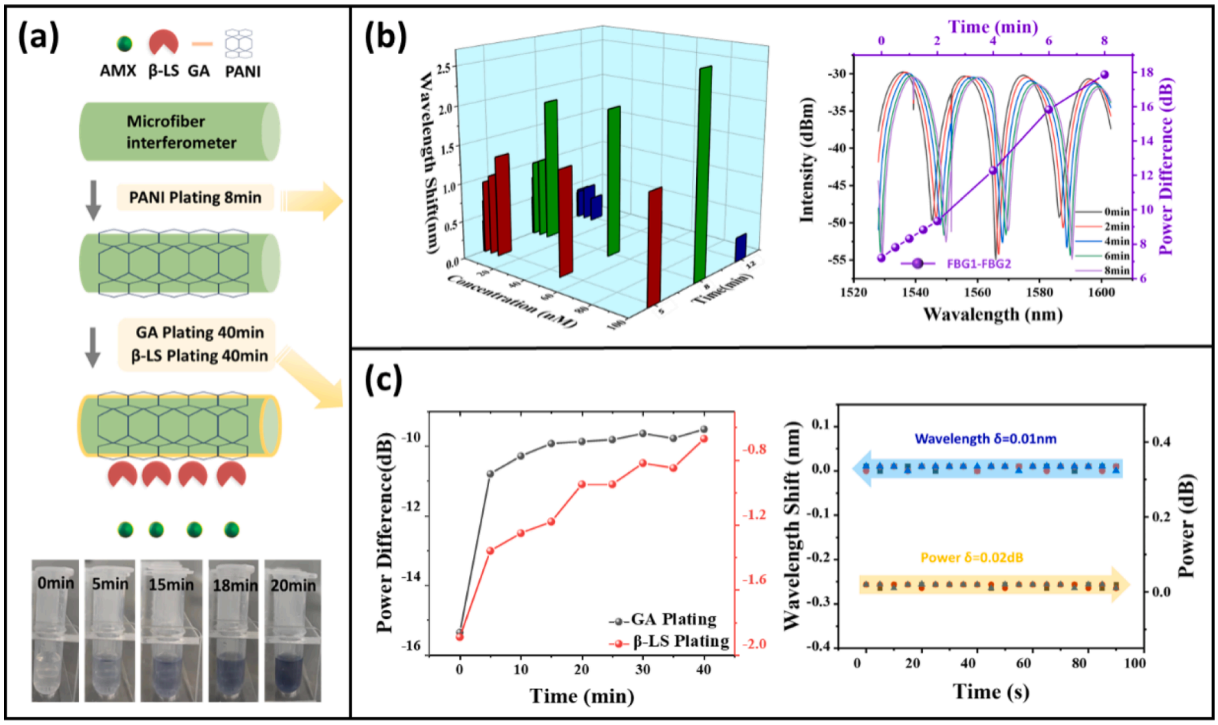

Fig. 4. (a) Diagram of the fabricated model of the MFI biosensor. (b) (left): selection of the time of the MFI coated with PANI. (right): the change relation of coating time with the power difference of FBGs and wavelength change of PANI-coated at 8 min. (c) (Left): Variation of coating time and power difference of FBGs about GA and β-LS. (right): Stability experiment of the full-fiber system biosensor.

phenomenon, where the color of the PANI solution changes from blue to green when the pH decreases, which induces a change in the RI around the PANI nanofiber-modified fiber. A similar-style all fiber system based on a microfiber interferometer coated a functional film and power changes of FBGs is proposed to realize for the specific detection of amoxicillin concentration.

3. Results and discussion

3.1. The performance of all-fiber systems with MFI and FBGs power variations

Experiments on the RI and temperature response of the MFI and FBGs power variations of the all-fiber system are performed. The interferogram of the all-fiber system is shown in Fig. 3 (a, top), where it can be seen that the two FBGs (The wavelengths of 1539.4 nm and 1551.55 nm) are located on either side of an interferometer dip (1542 nm). In order to simulate the spectral phenomenon, the RI of the all-fiber system is varied using different concentrations of NaCl solutions, and the RI values of these solutions are measured by a digital refractometer with an accuracy of 0.0002. When the RI around the all-fiber system changes, the interferometer wavelength is red-shifted, while the wavelength of the FBGs stays the same, and the reflective intensity of the two FBGs changes in the opposite trend. The changes in the Spectrum of the all-fiber system at RI of 1.3399 and 1.342 are shown in Fig. 3 (a, bottom), from which it can be seen that the MFI wavelengths are redshift. The FBGs wavelength are keeping constant but the FBG1 power is increased and the FBG2 power is decreased. The reflected power of the two FBGs is recorded using two OPMs and their power difference is calculated. The power changes of FBG1 and FBG2 for different RI are shown in Fig. 3(b, top), where the power of FBG1 decreases and the power of FBG2 increases when the RI increases. Fig. 3 (b, bottom, black) shows the wavelength variation of the MFI under different RI conditions, and the results show that the MFI wavelength is gradually redshifted during the experiment with the sensitivity of the RI of 952.7 nm/RIU. Fig. 3 (b, bottom, red) shows the variation of the power difference of the normalized FBG1-FBG2 under different RI conditions, and the results show that the power difference is gradually increasing during the experiment with the FBGs power different sensitivity of RI is 4199.6 dB/RIU. The change of FBGs power difference is more sensitive to RI than any single reflected power of FBG, and the change of FBGs power difference is more sensitive to RI than the change of MFI wavelength.

Temperature information is also important in RI measurements because thermo-optic and thermal expansion effects lead to changes in the spectrum and cause temperature cross-sensitivity [30]. In order to characterize the change in the temperature response of the all-fiber system, the all-fiber system is placed in a thermostat and the heating device varies from 30℃ to 90℃. The temperature performance of the all-fiber system is shown in Fig. 3(c). As the temperature increases, wavelength of the two FBGs are in redshift, as shown in Fig. 3 (c, top) the temperature response sensitivity of FBG1 and FBG2 are 0.01 nm/℃ and 0.08 nm/℃, which indicates that the temperature change has a small effect on the wavelength sensitivity of the FBGs. The temperature sensitivity for the difference in power of the two FBGs is 0.07 dB/℃, and Fig. 3 (c, bottom, black) shows the wavelength sensitivity of the MFI for different temperature conditions is −0.02 nm/℃. The all-fiber system eliminates temperature cross-sensitivity relative to RI sensitivity.

3.2. Fabrication of biosensors for all-fiber system

In order to achieve specific detection of AMX concentration, an all-fiber system with a microfiber optic interferometer based on PANI-coated functional films and FBGs power variation is proposed. Fig. 4 (a, top) shows the coating of the MFI throughout the experiment. In order to modify the optical fiber with PANI nanofibers[18], 50 mM of aniline and 50 mM of ammonium persulfate (APS) are reconstituted by adding them to 1 M of phosphoric acid, respectively. And then 1 mL of each of the reconstituted aniline and ammonium persulfate solutions are mixed to oxidize the aniline to OANI, and APS acted as the oxidizing agent for the redox polymerization in this process. During the

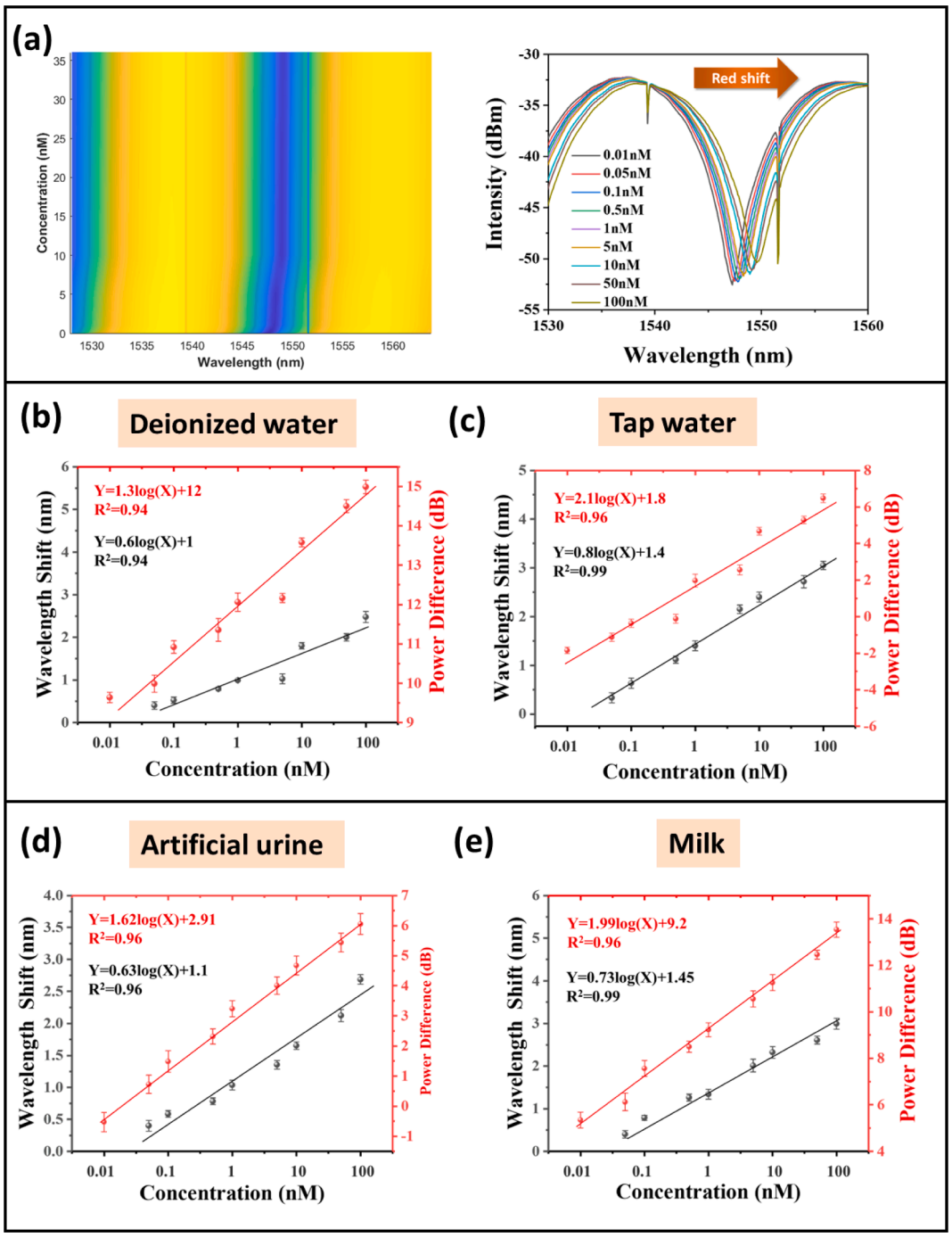

Fig. 5. (a) Interferogram of the biosensor detecting different concentrations of AMX. (b) Response calibration curves of the biosensor to detect different concentrations of AMX (prepared in deionized water). (c) Response calibration curves of the biosensor to detect different concentrations of AMX (prepared in tap water). (d) Response calibration curves of the biosensor to detect different concentrations of AMX (prepared in artificial urine) (e) Response calibration curves of the biosensor to detect different concentrations of AMX (prepared in milk).

experiment, it can be seen that the polymerization mixture solution gradually changed from colorless to light blue and finally to blue, which proved the oxidative polymerization of PANI, and the whole process is polymerized at room temperature for about 20 min, as shown in Fig. 4 (a, bottom).

The PANI obtained by polymerization is immobilized on MFI of an all-fiber system by in-situ growth method. The optical density of the PANI microfiber deposited on the MFI plays an important role in the sensitivity of the all-fiber system; the lower the coverage of PANI on the surface of MFI has lower sensitivity, whereas the higher the coverage has the higher sensitivity, due to the larger total surface area available for protonation. However, it should be noted that there is a tradeoff between PANI functional time and RI sensitivity (together with transmission loss). To determine the optimal time for the PANI functional membrane, the MFI is immersed in PANI solution for 5 min, 8 min, and 12 min. The results are shown in Fig. 4(b, left). In detail, the MFI after 5 min of PANI functional membrane (Red data) detected various concentrations of AMX (5 nM, 10 nM, 50 nM, and 100 nM), and the wavelength is shifted by 1.05 nm, 1.325 nm, 1.325 nm, and 1.39 nm, respectively. The MFI on PANI functional time of 12 min (Blue data) is

detected various concentrations of AMX (5 nM, 10 nM, 50 nM, and 100 nM), and the wavelength is shifted by 0.45 nm, 0.325 nm, 0.325 nm and 0.325 nm, respectively. The MFI after coating PANI functional membrane for 8 min (Green data) detected different concentrations of AMX (5 nM, 10 nM, 50 nM, and 100 nM), and the wavelength is shifted by 1.05 nm, 1.875 nm, 1.95 nm, and 2.625 nm, respectively. It can be concluded that 8 min is the optimal coating time, which not only can detect the larger concentration of AMX, but also the sensitivity maximum. Fig. 4 (b, right, purple) shows that the power difference of FBGs of the all-fiber system for coating 8 min is linear with time. During the coating process (8 min), the change of the interference spectrums is recorded by an OSA, which can be seen that the interference dips are in the regular redshift in Fig. 4 (b, right), proving that there is a PANI functional film attached to the MFI surface.

β-LS is immobilized on PANI-coated microfiber by covalent cross-linking with GA. During the experiments, the PANI-coated full-fiber system is incubated in 1 % (v/ v) GA aqueous solution for 40 min and is immobilized 120 IU/mL of β-LS (reconstituted in DI) on the MFI for 40 min. In Fig. 4 (c, left) the black line indicates the change of power difference of FBGs when GA is incubated on PANI-attached MIF for 40 min. In detail, the power difference changes 5.48 dB from 0 min to 20 min, and from 20 min to 40 min the power difference changes only 0.35 dB, which showing that the curves gradually became towards stability after GA incubated on MFI for 20 min. The red line indicates the change of power difference of FBGs after β-LS incubated on MIF with PANI/GA for 40 min. From 0 min to 20 min, the power difference of FBGs changes 0.94 dB, and from 20 min to 40 min the power difference changes only 0.28 dB, and it can be seen that the curve gradually became smooth when β-LS is incubated on MFI for 20 min. In order to demonstrate the stability of the biological system, the biosensor based on PANI/GA/β-LS is subjected for washing experiments in DI solution for 90 s. In Fig. 4(c, right), the results show that the interference spectrum is basically unchanged, and the wavelength of MFI error fluctuation is 0.01 nm. the power difference of FBGs changed to 0.02 dB. Finally, the full-fiber system biosensor based on PANI/GA/β-LS is successfully prepared and used for the next detection experiment.

3.3. Detection of amoxicillin

In this experiment, the response of PANI/GA/β-LS thin-film based functional biosensors to β-lactam antibiotics (AMX is chosen for this experiment) at different concentrations (0.01 nM-100 nM) in DI and tap water is investigated. During the experiments, AMX solutions with concentrations of 0.01 nM, 0.05 nM, 0.1 nM, 0.5 nM, 1 nM, 5 nM, 10 nM, 50 nM, and 100 nM are prepared. Specifically, an aqueous AMX solution of 100 nM is prepared and then diluted with DI to the final concentrations. During the detection process, starting from small concentrations, MFI based functional film is immersed in the AMX aqueous solution for 10 min, and the interference wave at final stabilization is selected as the most important data for this study. The wavelength change of the interference spectrum is recorded, and the transmission spectrum is shown in Fig. 5(a). Fig. 5(a, left) shows the wavelength response of the interference spectrum using PANI/GA/β-LS thin film functional biosensor to detect different concentrations of AMX. Fig. 5(a, right) shows the displacement change of the corresponding interference spectrum. It can be seen that the wavelength is gradually red-shifted as the concentration increases.

In this experiment we refer to the log function for converting the concentration of AMX added, then the relationship between the concentration of AMX and the wavelength shift is linear. Fig. 5(b) shows the calibration curves for the wavelength shift of MFI (black line) and the power difference change of FBGs (red line) in different concentrations of AMX solution (aqueous AMX solution prepared in DI). Each experiment is repeated three times under the same steps and conditions and analyzed with error bars. when the biosensor detects different concentrations of AMX, a linear calibration curve with a detection sensitivity of wavelength shift is 0.6 nm/nM. If the concentration of the detected substance is correct and the wavelength shift is known, the concentration of the analyte can be calculated by linear transformation. The average wavelength shift deviation of the three experiments is 0.01 nm, which is small within the acceptable range, and the main reason for the error is thermal noise. The theoretical detection limit can be calculated as LOD = 3σ/S, where σ is the standard deviation of the error measurement, which is 0.01 nm, and S is the slope of the calibration curve is 0.6 nm/nM [31], which is calculated to be LOD = 0.05 nM. A linear calibration curve with a detection sensitivity of power difference is 1.3 dB/nM, The theoretical detection limit LOD = 3σ/S = 0.04 nM, where σ = 0.02 dB and S = 1.3 dB/nM.

Everyday tap water is likely to contain β-lactam antibiotics, non-β-lactam antibiotics, or a mixture of several other organic and inorganic components. We select local tap water and configure it with different concentrations of AMX (0.01 nM −100 nM), and test the AMX solution in tap water using the same analytical method. To ensure that the experiments are not generated by chance, each experiment is performed three times and analyzed for errors. Fig. 5(c) shows the calibration curve of the wavelength change of MFI and the power difference change of FBGs (red line) of the sensor in tap water solutions with different concentrations of AMX. A linear calibration curve with a detection sensitivity of wavelength shift is 0.8 nm/nM, the theoretical detection limit LOD = 0.03 nM, and a detection sensitivity of power difference is 2.1 nm/nM, the theoretical detection limit of LOD = 0.02 nM. The Wavelength shift of the MFI and intensity variation of the FBGs in tap water will be higher than that detected in DI because tap water may contain a small amount of AMX impurities. Finally, we can detect the concentration of AMX by judging the change of wavelength or the change of power difference of the biosensor, and the lowest detection limit is 0.02 nM. Combining the above analysis and test results, it can be concluded that the functional biosensor based on the PANI/GA/β-LS thin film has high precision and superior stability for AMX, and detecting the concentration of AMX by the power change of FBG can reduce the cost of the system.

The practical application of the sensing system to test the detection sensitivity of different concentrations of amoxicillin in artificial urine and food (milk) is studied. During the experiment, 0.01 g of AMX is added to 1 mL of artificial urine and milk, respectively, for obtaining a 0.027 M solution of AMX, which is later diluted with DI to the target assay concentration. The concentration gradients are 0.01 nM, 0.05 nM, 0.1 nM, 0.5 nM, 1, 5 nM, 10 nM, 50 nM, and 100 nM. To ensure that the experiments are not generated by chance, we do repeatability experiments to analyze the errors. Fig. 5(d) shows the calibration curves for wavelength shift of MFI (black line) and power difference of FBGs (red line) in artificial urine with different concentrations of AMX. The wavelength shift detection sensitivity is 0.63 nm/nM, with the theoretical detection limit LOD = 0.04 nM. The power difference detection sensitivity is 1.62 dB/nM, with the theoretical detection limit LOD = 0.03 nM. Fig. 5(e) shows the calibration curves for the wavelength change of MFI (black line) and the power difference change of FBGs (red line) with different concentrations of AMX in milk. The sensitivity of wavelength shift detection is 0.73 nm/nM, with the theoretical detection limit LOD = 0.04 nM. The sensitivity of power difference detection is 1.99 dB/nM, with the theoretical detection limit LOD = 0.03 nM. An all-fiber-optic system for rapid detection of antibiotic concentration has been verified successfully in food samples and artificial urine.

3.4. Specific detection

The specificity of the biosensor is an important criterion for evaluating the performance of the biosensor. The biosensor selectively is studied some non-β-lactam antibiotics such as erythromycin (macrolide), levofloxacin (fluoroquinolone), doxycycline (tetracycline), rifampicin (anti-tuberculosis), 5-fluorocytosine (antifungal), tobramycin (aminoglycoside). The experimental procedure is carried out by

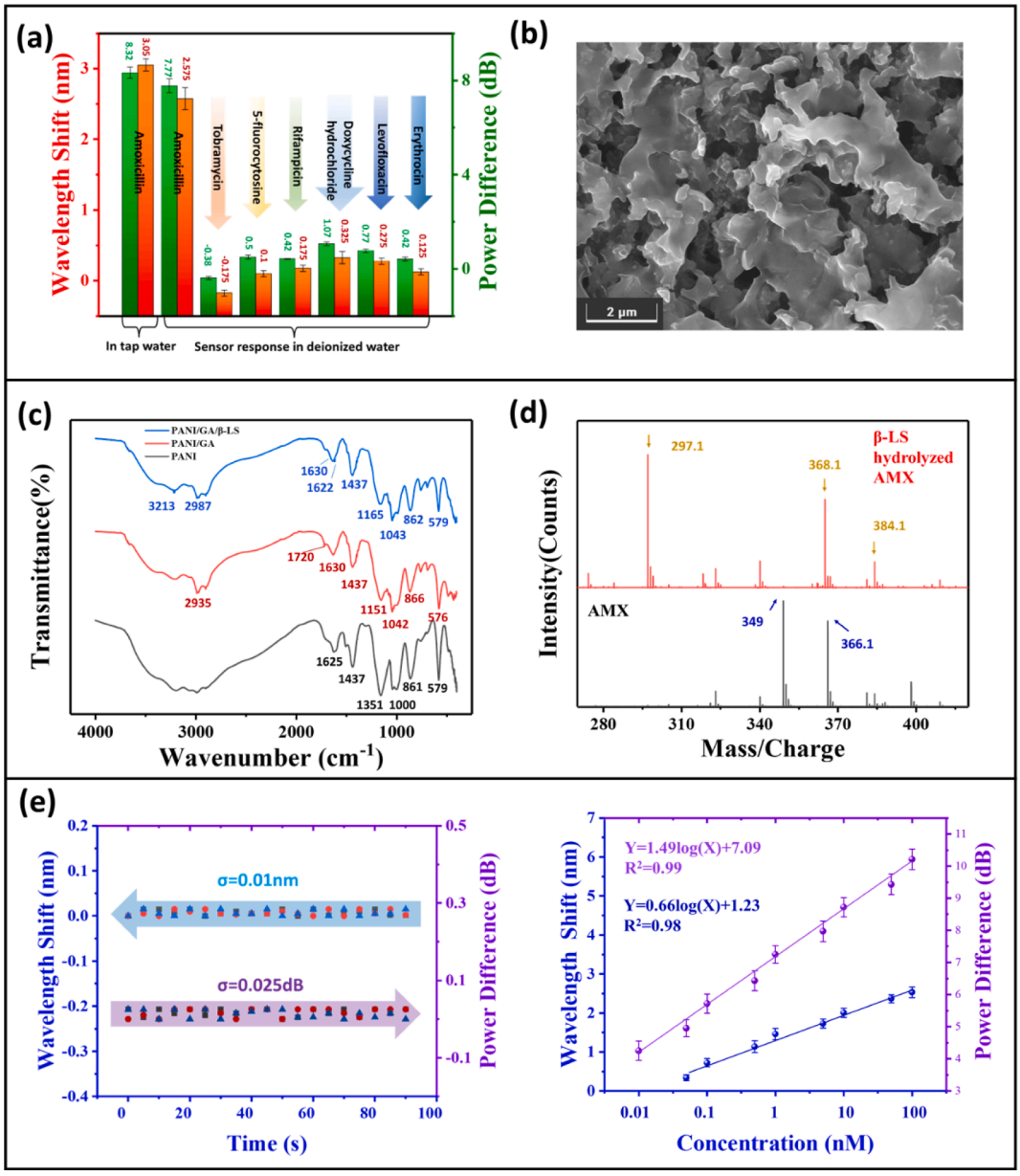

Fig. 6. (a) Specific response of the biosensor based on PANI/GA/β-LS film to different substances (AMX, Tobramycin, 5-fluorocytosine, Rifampicin, Doxycycline hydrochloride, Levofloxacin, Erythromycin). (b) SEM analysis of PANI coated optical fiber. (c) FTIR analysis of PANI, PANI/GA, and PANI/GA/β-LS. (d) Mass spectra of AMX and β-LS hydrolyzed AMX (yellow arrows indicate hydrolysis peaks). (e) The results of the sensor stability and detection sensitivity experiments obtained by storing the biosensors at room temperature for 21 days. (For interpretation of the references to color in this figure legend, the reader is referred to the web version of this article.)

configuring different concentrations of aqueous solutions (0.01 nM-100 nM, obtained by dilution in DI) for the different substances. This detecting process uses the same analytical method used in Section 3.3 for repeating the experiment three times then performing an error analysis and selecting the final stabilized data as the experimental data. Fig. 6(a) shows the response of the biosensor to different substances. The results show that the wavelength shift and power difference changes of AMX, Tobramycin, 5-fluorocytosine, Rifampicin, Doxycycline hydrochloride, Levofloxacin, and Erythromycin, in DI solution are 2.575 nm (7.77 dB), −0.175 nm (-0.38 dB), 0.1 nm (0.5 dB), 0.175 nm (0.42 dB), 0.325 nm (1.07 dB), 0.275 nm (0.77 dB), and 0.125 nm (0.42 dB), respectively, and the changes in the wavelength shifts and power differences for AMX in tap water are 3.05 nm (8.32 dB). This indicates that the response of the biosensor to AMX is much higher than that of other substances, and it can be determined that the response of the sensor is for the enzymatic hydrolysis of specific β-lactam antibiotics and that the sensor has good specificity for AMX.

The morphology of the PANI coated optical fiber is analyzed by field emission SEM, as shown in Fig. 6(b). It can be seen that the PANI is uniformly distributed on the microfiber After that, the PANI and GA immobilized PANI (short for PANI/GA), and β-LS immobilized PANI/GA (short for PANI/GA/β-LS) are subjected to FTIR analysis, respectively, as shown in Fig. 6(c). The black line is the FTIR of PANI, from which it can be seen that the peaks at 1625 cm^{-1} and 1437 cm^{-1} correspond to the C═C stretching vibrations of the benzene and quinone rings of polyaniline. The sharp peaks at 1351 cm^{-1} and 1000 cm^{-1} are C—N extensions of PANI secondary aromatic amines [32]. The peak at 861 cm^{-1} is the stretching of the C—C bond of the alkyl chain of PANI, and the peak at 817 cm^{-1} is related to the bending and vibration of C—H in PANI [18]. The red line indicates the FTIR of PANI/GA, and it can be seen that

Table 1
Comparison of the performance of different methods for the detection of antibiotics.

Method	Receptor	Experimental LoD	range	Cost	Publication date	Ref
Colorimetric	Quercetagetin coated AgNPs	4.46×10^{-6} M	10×10^{-6} M -95×10^{-6}M	medium	2018	[13]
Colorimetric	Nitro blue tetrazolium	$2.6x10^{-6}$M	$8x10^{-6}$M $-50x10^{-6}$ M	medium	2023	[14]
Electrochemical	Aptamer	1×10^{-6} M	5×10^{-6} M -5000×10^{-6} M	high	2018	[11]
Electrochemical	β-lactamase	0.79×10^{-7} M	0.26×10^{-6} M -0.66×10^{-6} M	high	2014	[12]
Electro-optical sensor	Pseudomonas putida TSh-18	$1.4x10^{-6}$M	$1.4x10^{-6}$ M –$1.8\ x10^{-3}$M	high	2021	[15]
Surface plasmon resonance sensor	Molecularly imprinted polymer	0.073×10^{-9}M	0.1×10^{-9} M -2.6×10^{-9}M	medium	2018	[16]
Surface-enhanced Raman spectroscopy sensor	Rhodamine 6G	1×10^{-6} M	10^{-1} M – 10^{-6}M	medium	2019	[17]
U-shaped sensor	Enzyme-β-lactamase	0.18×10^{-9} M	0.18×10^{-9} M -1800×10^{-9} M	medium	2021	[18]
All-fiber biosensors optic sensor	Enzyme-β-lactamase	0.05×10^{-9} M	0.01×10^{-9} M -100×10^{-9} M	low	2023	this work

the modification of PANI with GA does not change much on most of the peaks. However, the additional sharp peaks are observed at 1720 cm^{-1} and 2935 cm^{-1} due to -C═O stretching and –CH stretching of the free aldehyde group, which confirming the modification of PANI with GA [33]. The blue line indicates the FTIR of the PANI/GA/β-LS modified fiber. The peak at 1622 cm^{-1} is the C═O vibration of the β-LS amide bond, and the peak at 3213 cm^{-1} is the amide band of β-LS [34].

High-resolution mass spectrometry analysis of AMX and β-LS hydrolyzed AMX is performed. The results are shown in Fig. 6(d). The peak of AMX molecule (molecular weight 365.4) is shown as the black line, and a peak at *m/z* 349 appeared due to NH_2 loss $[M-NH_2+H]+$. The peak at *m/z* 366.1 corresponds to the sodium adduct $[M-NH_2+Na]+$ of the NH_2 eliminated molecular ion. The mass spectra of β-LS hydrolyzed AMX are shown as the red line. It can be observed that the peak at *m/z* 349 disappears when β-LS is combined with AMX. The new peak at *m/z* 368.1 is hydrogen $[Mhyd\text{-}NH_2+H]+$ of the hydrolyzed NH_2 elimination molecular ion, and the peak at *m/z* 384.1 is sodium $[MhydNH_2+Na]+$ adduct of hydrolyzed NH_2. The peak at *m/z* 297.1 is the decarboxylated form of the molecular ion eliminated by hydrolyzed NH_2 [18]. The above analysis confirms that AMX can be hydrolyzed by β-LS and form acidic by-products. Table 1 shows the comparison of the performance of antibiotic detection by different methods. In comparison, our sensor is simple to fabricate, easy to operate, with stable performance and high sensitivity.

The effect of the biosensors long placed in some conditions on the stability and detection sensitivity is experimentally verified. During the experiment, the fabricated biosensors store at room temperature and tested the stability and sensitivity on the twenty-first day and the obtain experimental data are shown in Fig. 6(e). Fig. 6 (e, left) shows the wavelength change and power difference over time for the sensor washed in DI for 3 min. The wavelength fluctuation of 0.01 nm and the power difference fluctuation of 0.025 dB do not change significantly compared to the first day (0.01 nm (wavelength fluctuation), 0.02 dB (power difference fluctuation)). Fig. 6 (e, right, purple line) shows the fitted curve of the sensor power difference with concentration is 1.49 dB/nM, and Fig. 6 (e, right, blue line) shows the fitted curve of the sensor wavelength change with concentration is 0.66 nm/nM. From the experimental data, it can be seen that the stability of water washing on the twenty-first day remained basically unchanged compared to the first day (1.3 dB/nM (power difference sensitivities), 0.6 nm/nM (wavelength change sensitivities)), It can be concluded that this sensing system very good stability for detecting biosensor performance.

4. Conclusion

A fiber optic biosensing system capable of determining AMX concentration based on MFI wavelength and FBGs power difference variation is developed. The sensing system by the same calibration technique can detect antibiotic concentrations in different substances (tap water, milk and artificial urine). Detecting AMX in the concentration range of 0.01–100 nM, experimental results show that MFI wavelength variation detection sensitivity is 0.6 nm/nM, and FBGs power difference change sensitivity of 1.3 dB/nM, with a detection limit LOD = 0.04 nM in real food and urine samples. The developed biosensing system are stable and specific, and this biosensing technology has great potential for monitoring antibiotic concentrations in food and water. It is also of great practical value for detecting antibiotic concentrations in ordinary wastewater treatment plants and can also be used to monitor the presence of β-lactam antibiotics in tap water and their removal during treatment.

CRediT authorship contribution statement

Dandan Sun: Formal analysis, Funding acquisition, Investigation, Project administration, Writing – review & editing. **Zifan Hou:** Data curation, Formal analysis, Writing – original draft. **He Yan:** Data curation, Formal analysis. **Yukun Yang:** Investigation, Methodology. **Guanjun Wang:** Investigation, Supervision. **Jizhou Wu:** Project administration, Supervision. **Jie Ma:** Funding acquisition, Project administration, Supervision.

Declaration of competing interest

The authors declare that they have no known competing financial interests or personal relationships that could have appeared to influence the work reported in this paper.

Data availability

Data will be made available on request.

Acknowledgments

This work was supported by National Natural Science Foundation of China (62005147, 62175054, 32072301, 62175140); International Cooperation and Exchange of the National Natural Science Foundation of China (62020106014).

References

[1] K.L. Tang, N.P. Caffrey, D.B. Nóbrega, S.C. Cork, P.E. Ronksley, H.W. Barkema, A. J. Polachek, H. Ganshorn, N. Sharma, J.D. Kellner, W.A. Ghali, Restricting the use

of antibiotics in food-producing animals and its associations with antibiotic resistance in food-producing animals and human beings: a systematic review and meta-analysis, Lancet. Planetary Health 1 (8) (2017) e316–e327, https://doi.org/10.1016/S2542-5196(17)30141-9.
[2] A.A. Oladipo, S. Derakhshan Oskouei, M. Gazi, Metal-organic framework-based nanomaterials as opto-electrochemical sensors for the detection of antibiotics and hormones: A review, Beilstein J. Nanotechnol. 14 (1) (2023) 631–673, https://doi.org/10.3762/bjnano.14.52.
[3] M.J. Pons, J. Ruiz, Current trends in epidemiology and antimicrobial resistance in intensive care units, J. Emergency and Crit. Care Med., 3 (2019) 5. 10.21037/jeccm.2019.01.05.
[4] P.K. Mutiyar, A.K. Mittal, Occurrences and fate of selected human antibiotics in influents and effluents of sewage treatment plant and effluent-receiving river Yamuna in Delhi (India), Environ. Monit. Assess. 186 (1) (2014) 541–557, https://doi.org/10.1007/s10661-013-3398-6.
[5] K. Kümmerer, Drugs in the environment: emission of drugs, diagnostic aids and disinfectants into wastewater by hospitals in relation to other sources–a review, Chemosphere 45 (2001) 957–969, https://doi.org/10.1016/S0045-6535(01)00144-8.
[6] H. Roman, T. Thomas, H. Klaus, Occurrence of antibiotics in the aquatic environment, Sci. Total Environ. 225 (1999) 109–118, https://doi.org/10.1016/S0048-9697(98)00337-4.
[7] M.G. Pikkemaat, Microbial screening methods for detection of antibiotic residues in slaughter animals, Anal. Bioanal. Chem. 395 (4) (2009) 893–905, https://doi.org/10.1007/s00216-009-2841-6.
[8] M.T. Meyer, J.E. Bumgarner, J.L. Varns, J.V. Daughtridge, E.M. Thurman, K. A. Hostetler, Use of radioimmunoassay as a screen for antibiotics in confined animal feeding operations and confirmation by liquid chromatography/mass spectrometry, Sci. Total Environ. 248 (2–3) (2000) 181–187, https://doi.org/10.1016/s0048-9697(99)00541-0.
[9] K. Kumar, A. Thompson, A.K. Singh, Y. Chander, S.C. Gupta, Enzyme-linked immunosorbent assay for ultratrace determination of antibiotics in aqueous samples, J. Environ. Qual. 33 (1) (2004) 250–256, https://doi.org/10.2134/jeq2004.2500.
[10] J. Tschmelak, G. Proll, G. Gauglitz, Optical biosensor for pharmaceuticals, antibiotics, hormones, endocrine disrupting chemicals and pesticides in water: Assay optimization process for estrone as example, Talanta 65 (2) (2005) 313–323, https://doi.org/10.1016/j.talanta.2004.07.011.
[11] Z.G. Yu, R.Y. Lai, A reagentless and reusable electrochemical aptamer-based sensor for rapid detection of ampicillin in complex samples, Talanta 176 (2018) 619–624, https://doi.org/10.1016/j.talanta.2017.08.057.
[12] Y. Wu, L. Tang, L. Huang, Z. Han, J. Wang, H. Pan, A low detection limit penicillin biosensor based on single graphene nanosheets preadsorbed with hematein/ionic liquids/penicillinase, Mater. Sci. & Eng. C, Mater. Biol. Appl. 39 (2014) 92–99, https://doi.org/10.1016/j.msec.2014.02.012.
[13] N.U. Ain, I. Anis, F. Ahmed, M.R. Shah, S. Parveen, S. Faizi, S. Ahmed, Colorimetric detection of amoxicillin based on quercetagetin coated silver nanoparticles, Sens. Actuators B 265 (2018) 617–624, https://doi.org/10.1016/j.snb.2018.03.079.
[14] N. Sethu, S. Krishnakumar, V. Mitra, C.K. Tagad, R. Vyas, Design and development of a novel colorimetric assay and a portable optical system for the detection of aminoglycoside antibiotics, Sensors and Actuators Reports 14 (2023), 100151, https://doi.org/10.1016/j.snr.2023.100151.
[15] O.I. Guliy, S.S. Evstigneeva, V.D. Bunin, Bacteria-based electro-optical platform for ampicillin detection in aquatic solutions, Talanta 225 (2021), 122007, https://doi.org/10.1016/j.talanta.2020.122007.
[16] A.G. Ayankojo, J. Reut, A. Öpik, A. Furchner, V. Syritski, Hybrid molecularly imprinted polymer for amoxicillin detection, Biosens. Bioelectron. 118 (2018) 102–107. https://doi:10.1016/j.bios.2018.07.042.
[17] D. Gao, X. Yang, P. Teng, Z. Liu, J. Yang, D. Kong, J. Zhang, M. Luo, Z. Li, F. Tian, L. Yuan, Optofluidic in-fiber integrated surface-enhanced Raman spectroscopy detection based on a hollow optical fiber with a suspended core, Opt. Lett. 44 (21) (2019) 5173–5176, https://doi.org/10.1364/OL.44.005173.
[18] P. Nag, K. Sadani, S. Mohapatra, S. Mukherji, S. Mukherji, Evanescent Wave Optical Fiber Sensors Using Enzymatic Hydrolysis on Nanostructured Polyaniline for Detection of β-Lactam Antibiotics in Food and Environment, Anal. Chem. 93 (4) (2021) 2299–2308, https://doi.org/10.1021/acs.analchem.0c04169.
[19] V.R. Bhardwaj, K. Kishor, A.C. Sharma, Tapered optical fiber geometries and sensing applications based on Mach-Zehnder Interferometer: A review, Opt. Fiber Technol. 58 (2020), 102302, https://doi.org/10.1016/j.yofte.2020.102302.
[20] Y. Li, J. Zhang, Y. Wang, H. Du, J. Wu, W. Liu, F. Mei, J. Ma, L. Xiao, S. Jia, Atom-optically synthetic gauge fields for a noninteracting Bose gas, Light Sci. Appl. 11 (1) (2022) 13, https://doi.org/10.1038/s41377-021-00702-7.
[21] Y. Huang, Z. Tian, L.P. Sun, D. Sun, J. Li, Y. Ran, B.O. Guan, High-sensitivity DNA biosensor based on optical fiber taper interferometer coated with conjugated polymer tentacle, Opt. Express 23 (21) (2015) 26962–26968, https://doi.org/10.1364/OE.23.026962.
[22] P. Gong, X. Li, X. Zhou, Y. Zhang, N. Chen, S. Wang, S. Zhang, Y. Zhao, Optical fiber sensors for glucose concentration measurement: A review, Opt. Laser Technol. 139 (2021), 106981, https://doi.org/10.1016/j.optlastec.2021.106981.
[23] D. Sun, Y. Fu, Y. Yang, Label-free detection of breast cancer biomarker using silica microfiber interferometry, Opt. Commun. 463 (2020), 125375, https://doi.org/10.1016/j.optcom.2020.125375.
[24] D. Srivastava, R. Bhatnagar, A. Kumar, V. Parmar, Intensity modulation using chirped fiber bragg grating as an edge filter for temperature sensing, Microw. Opt. Technol. Lett. 56 (2014) 2913–2915, https://doi.org/10.1002/mop.28737.
[25] C. Zhang, S. Xu, J. Zhao, H. Li, H. Bai, C. Miao, Multipoint refractive index and temperature fiber optic sensor based on cascaded no core fiber-fiber Bragg grating structures, Opt. Eng. 56 (2017), 027102, https://doi.org/10.1117/1.OE.56.2.027102.
[26] Y. Wang, H. Du, Y. Li, F. Mei, Y. Hu, L. Xiao, J. Ma, S. Jia, Testing universality of Feynman-Tan relation in interacting Bose gases using high-order Bragg spectra, Light Sci. Appl. 12 (1) (2023) 50, https://doi.org/10.1038/s41377-023-01103-8.
[27] S.H.K. Yap, Y.H. Chien, R. Tan, A.R. Bin Shaik Alauddin, W.B. Ji, S.C. Tjin, K. T. Yong, An Advanced Hand-Held Microfiber-Based Sensor for Ultrasensitive Lead Ion Detection, ACS Sensors 3 (12) (2018) 2506–2512, https://doi.org/10.1021/acssensors.8b01031.
[28] A. Srivastava, R. Kumar, M. Kumar, BlaPred: Predicting and classifying β-lactamase using a 3-tier prediction system via Chou's general PseAAC, J. Theor. Biol. 457 (2018) 29–36, https://doi.org/10.1016/j.jtbi.2018.08.030.
[29] G.G. Wallace, G.M. Spinks, L.A. Kane-Maguire, P.R. Teasdale, Conductive Electroactive Polymers: Intelligent Polymer Systems 3 (2009) 263, https://doi.org/10.1201/9781420067156.
[30] E. Li, X. Wang, C. Zhang, Fiber-optic temperature sensor based on interference of selective higher-order modes, Appl. Phys. Lett. 89 (2006), 091119, https://doi.org/10.1063/1.2344835.
[31] L. Liang, L. Jin, Y. Ran, L.P. Sun, B.O. Guan, Fiber Light-Coupled Optofluidic Waveguide (FLOW) Immunosensor for Highly Sensitive Detection of p53 Protein, Anal. Chem. 90 (18) (2018) 10851–10857, https://doi.org/10.1021/acs.analchem.8b02123.
[32] N.P. Chauhan, R. Ameta, R. Ameta, S.C. Ameta, Thermal and conducting behaviour of emeraldine base (EB) form of polyaniline (PANI), Indian J. Chem. Technol. 18 (2011) 118–122. https://api.semanticscholar.org/CorpusID:35879144.
[33] A.D. Chowdhury, A.K. De, C.R. Chaudhuri, K. Bandyopadhyay, P. Sen, Label free polyaniline based impedimetric biosensor for detection of E. coli O157:H7 Bacteria, Sens. Actuators B 171–172 (2012) 916–923, https://doi.org/10.1016/j.snb.2012.06.004.
[34] D. Usoltsev, V. Sitnikova, A. Kajava, M. Uspenskaya, Systematic FTIR Spectroscopy Study of the Secondary Structure Changes in Human Serum Albumin under Various Denaturation Conditions, Biomolecules 9 (8) (2019) 359, https://doi.org/10.3390/biom9080359.